Scaling and structure in isotropic turbulence

Javier Jiménez

School of Aeronautics, Universidad Politécnica, 28040 Madrid, Spain, *and*
Centre for Turbulence Research, Stanford U., Stanford, CA 94305, USA

F. Moisy, P. Tabeling, H. Willaime

Laboratoire de Physique Statistique, Ecole Normal Supérieur, 24 rue Lhomond, 75231 Paris, France

1   Introduction

An especially intriguing aspect of turbulence is the interplay between structure and statistics. It is tempting to conclude that turbulent flows, because of many degrees of freedom,should be studied statistically, and that the limit theorems for the probability distributions should apply. The earliest theoretical results on the subject were indeed based on postulating 'structureless' models and applying to them scaling laws (Kolmogorov 1941) but, while it works in some approximation, it is known that this description is incomplete. Deterministic structures exist both at the largest scales (Brown and Roshko 1974) and at the smallest ones (Batchelor and Townsend 1949). Less is known about the intermediate length scales, and the study of their structure has traditionally been done statistically, in terms of the 'anomalous' scaling of the difference of the velocities at two points. The basic model in this range is the self-similar multiplicative cascade, which we will briefly discuss below (see Frisch, 1994 for a summary), but the main subject of this paper is the characterization of the inertial-range structures, if they can be shown to exist.

Anomalous scaling is, after all, probably the reflection of coherent structures within the inertial range of scales, but their study is complicated by experimental difficulties. The large-scale coherent structures are easily visualized, since they span the flow, while those at the smallest scales manifest themselves by strong gradients which can also be easily extracted from the velocity signals. None of those observational advantages are available in the inertial range, where structures are too small, and probably too numerous, to be readily apparent in visualizations of the velocity field, and also too weak to be seen in those of the gradients (see however the visualizations by Hosokawa, Oide and Yamamoto 1997, and by Porter, Woodward and Pouquet 1998).

In the next section we discuss our motivation for reconsidering the theory of the turbulent cascade. This is followed by the analysis of experimental velocity data, first of their coarse-grained dissipation, and latter of the conditional distributions of the velocity increments and of band-pass filtered velocities. Discussions and conclusions are finally offered in §6.

2 Multiplicative cascades and blocking

The concept of cascade was probably first explicitly introduced by Richardson (1922) to describe high-Reynolds number turbulence. Kolmogorov (1941) made it quantitative, on the implicit assumption that the velocity fluctuations were small enough for all the points in the flow to be described in terms of uniform characteristic scales. His later introduction of intermittency corrections (Kolmogorov 1962) improved on this approximation, but still assumed a uniform cascade in the sense that the only effect of local fluctuations was to introduce a locally variable velocity scale. It was pointed out by Jiménez and Wray (1998) and Jiménez (2000) that more complicated effects are possible.

Out of the many possible cascade models, self-similar multiplicative processes were first applied to turbulent flows by Gurvich and Yaglom (1967), and in more detail by Novikov (1971, 1990), although they were already implicit in the original Kolmogorov (1962) paper. Recent reviews are due to Meneveau and Sreenivasan (1991), Nelkin (1994) and Sreenivasan and Stolovitzky (1995). We will briefly summarize the basic ideas.

Consider a positive variable, v_n, that is assumed to cascade in discrete steps. Assume that the cascade is locally deterministic, which was defined by Jiménez (2000) as one in which the probability distribution of the cascading variable at one point, $p_n(v_n)$, depends only on its value at the previous step,

$$p_{n+1}(v_{n+1}) = \int p_t(v_{n+1}|v_n; n) p_n(v_n) \, \mathrm{d}v_n. \tag{2.1}$$

This is in contrast to more complicated functional dependences, such as on the values of v_n in some extended spatial neighbourhood, or on several previous cascade stages. This assumption intuitively implies that v_{n+1} evolves faster, or on a smaller scale, than v_n, and is in some kind of equilibrium with its precursor. If the cascade is deterministic in this sense, v_n can be represented as a product

$$v_n = x_n x_{n-1} \cdots x_1 u_0. \tag{2.2}$$

of factors, $x_n = v_n/v_{n-1}$, which are statistically independent of one another.

If moreover the underlying process is invariant to scaling transformations of v it should also be true that the transition probability density function has the form

$$p_t(v_{n+1}|v_n) = v_n^{-1} w(v_{n+1}/v_n), \tag{2.3}$$

It can easily be shown that local deterministic self-similar cascades lead naturally to intermittent distributions, in the sense that the high-order flatness factors for v_n become arbitrarily large as n increases, implying that arbitrarily strong, although rare, events inevitably appear at the later stages of the cascade.

If (2.3) does not depend explicitly on the cascade stage, these assumptions lead to power laws for the statistical moments of the pdfs, and to the theory of multifractal probability distributions. In particular the pdfs of v_n vary with the cascade step n in well-defined manner that depends only on the distribution, w, of the 'breakdown' coefficients x. The application of this theory to turbulence is usually justified by the invariance of the Euler equations to scaling transformations (Frisch 1994) but, although this addresses (2.3), it says nothing about the locality hypothesis (2.1).

It was pointed out by Jiménez (2000) that locality is unlikely to be satisfied in multiplicative cascades involving fields. The reason is that each cascading step, presumably an instability of some structure, is bound to be controlled at least partly by the background fluctuations, which introduce a spatially global scale v'_n. The break-up of a given eddy is then controlled by two velocity scales, its own intensity and the global fluctuation level, and self-similarity is broken.

Consider for example the decay of a large-scale vortex in a turbulent flow. As long as its vorticity is of the same order as that of the background its decay is controlled by the outside perturbations, which for example fix the time scale of the break-up. One of the consequences of the random cascade process is however that some of resulting vortices will be more intense than others and, as noted before, this will eventually lead to some structures which are much stronger than the average. Those strong structures are no longer subject to the influence of the background, and they in essence decouple from it. In some sense the cascade is 'blocked' for them, although all that we can conclude without going into the specific physics of a particular cascade process is that the breakdown of the weak and of the strong structures will be different, and that the flow will eventually differentiate into two distinct components. Simple models for cascades displaying such nonlinear blocking were given by Jiménez (2000), who also argued that, for the reasons sketched above, it is an almost inevitable consequence of applying random multiplicative cascades to fields. Such blocked cascades do not lead to power-law behaviours for the statistics.

In the particular case of vorticity in Navier-Stokes turbulence, it had been previously argued by Jiménez and Wray (1998) that the compact dissipation-range vortex filaments observed in many turbulent flows (Siggia 1981, Jiménez *et al.* 1993, Jiménez 1998) are in fact examples of such a blocked component of the standard Kolmogorov (or multifractal) cascade, which decouple from the background turbulent flow by virtue of their large internal vorticity.

3 Experimental setup

To test these theoretical ideas we have analyzed experimental data of approximately isotropic turbulence at three different Reynolds numbers.

The set-up is the same as that described by Zocchi *et al.* (1994), Tabeling *et al.* (1996), Belin *et al.* (1997) and Moisy, Tabeling and Willaime (1999). The flow is confined to a cylinder limited axially by disks equipped with blades rotating in opposite directions at approximately equal angular velocities. The disks are driven by DC motors modified to work at low temperatures, whose rotation speeds are accurately measured by analyzing the frequency content of the electrical current supply. The cylindrical working volume in which turbulence takes place is 20 cm in diameter, and 13.1 cm in height. The whole system is enclosed in a larger cylindrical vessel in thermal contact with a liquid helium bath, and is filled with helium gas at controlled pressure. Its temperature is kept constant between 4.2 and 6.5 K, with a long term stability better than 1 mK. Under those conditions the kinematic viscosity of the gas is typically between $10^{-3} - 10^{-2}$ cm^2/s, which is considerably below that of most conventional fluids. Far from the blades and away from the walls the flow behaves as a confined circular mixing layer (Zocchi *et al.* 1994), although the wall region is more complicated. For the data sets used in this paper the probe is located 4.7 cm from the mid-plane of the system, and 6.5 cm from the cylinder axis. This corresponds to the outer part of the mixing layer, which is more likely to have simple properties and where the presence of a substantial mean flow justifies the use of Taylor's hypothesis.

Velocity measurements are performed with a 'hot'-wire anemometer, whose sensor is a 7 μm thick carbon fibre stretched across a rigid frame. A metallic layer, 1000 A thick, covers the fibre everywhere except on a spot at the centre, 7 μm long, which defines the active length of the probe. The time response of the probe was analyzed by Tabeling *et al.* (1996). It depends on various factors, such the overheat ratio, but it is typically on the order of 2 μs. The sensor is unconventionally short but, owing to the thermal characteristics of carbon, no substantial enhancement of thermal inertia is to be expected. It was shown in the references given above that King's law accurately applies to the sensors in the range of operating conditions used in the experiments. Their directionality is bound to be poor but, because of the presence of a non-zero mean velocity, the measured fluctuations are predominantly longitudinal, and will be consider so in the rest of the paper.

The voltage from the anemometer is low-pass filtered, digitized and recorded. The reduction to velocity is done during the analysis, and time intervals are converted to lengths using Taylor's approximation with the overall mean velocity, $\Delta x = -\overline{U}\Delta t$. We consider three data sets, summarized in table 1. They are sampled at the Kolmogorov passing frequency, $\overline{U}/\eta$, and restricted to Reynolds numbers which are low enough for the dissipative range of scales to be well resolved. The three sets span a full decade of microscale Reynolds

	Re_λ	L_ε/η	$\Delta x/\eta$	$u'/\overline{U}$	N	L/L_ε
- - - -	155	2.5×10^2	1.6	0.20	1.4×10^7	8.8×10^4
—·—	760	2.8×10^3	1.8	0.22	3.7×10^7	2.5×10^4
——	1600	8.4×10^3	1.5	0.21	3.7×10^7	6.5×10^3

Table 1.- Characteristics of the three data sets used in this paper. u' is the one-component r.m.s. velocity fluctuation intensity, and $\overline{U}$ is the mean longitudinal velocity. The total number of samples in the set is N, which corresponds to a total sample length L. The sampling distance, using Taylor's hypothesis, is Δx. The globally averaged energy dissipation ϵ is used to compute the integral length, $L_\varepsilon = \epsilon/u'^3$, and the Kolmogorov length scale η. Line types are consistently used in the figures.
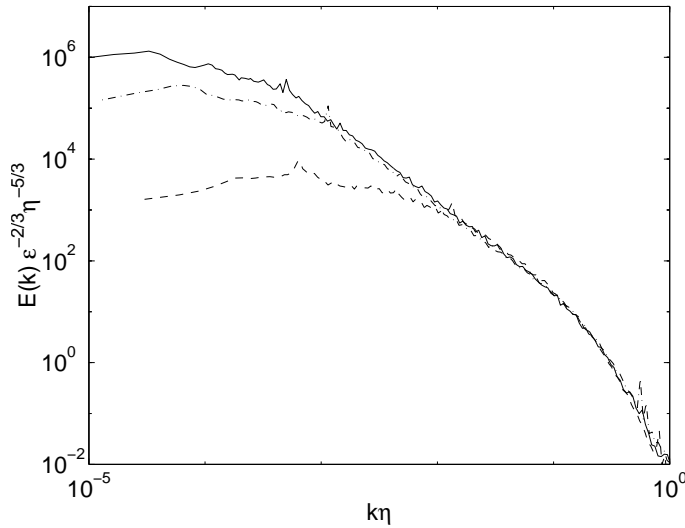

Figure 1.- One-dimensional power spectra of the three data sets analyzed in this paper. Line types as in table 1.

numbers, and the spectrum at the highest Reynolds number, shown in figure 1, presents almost three orders of magnitude of $k^{-5/3}$ power law. We will consider this to be the inertial range, although alternative characterizations are discussed by Moisy, Tabeling and Willaime (1999).

4 The breakdown coefficients for the dissipation

The usual scaling analysis of the coarse-grained surrogate dissipation,

$$\varepsilon_{\Delta x} = \frac{1}{\Delta x} \int_{x-\Delta x/2}^{x+\Delta x/2} (\partial_x u)^2 \, \mathrm{d}x, \tag{4.1}$$

was done first (Meneveau and Sreenivasan 1991). The pdfs of the centred breakdown coefficients

$$q_{2\Delta x} = \frac{1}{2}\varepsilon_{\Delta x}/\varepsilon_{2\Delta x}, \tag{4.2}$$

are bell-shaped in the inertial range, as previously reported by Van Atta and Yeh (1975) and by Chhabra and Sreenivasan (1992), but they become less so, and even concave, at the dissipative scales (see figure 2-*a*). Somewhat surprising, the shapes of the distributions vary continuously with the averaging scale, becoming more concentrated as the scale is made larger. This contradicts the conclusions of the two papers mentioned above, which were that the distributions are universal in the inertial range, and which have often been cited as experimental corroboration for the existence of a self-similar dissipative cascade. In fact, in spite of their own conclusions, the data of Van Atta and Yeh (1975) clearly show that their distributions vary with scale. They propose as a measure of the shape of the pdfs their value $p_{0.5}$ at $q = 0.5$. These values are plotted in figure 2(b), and it is clear that the same logarithmic trend is observed in their experiment as in ours. Chhabra and Sreenivasan (1992) published plot is small and difficult to read, and suggest $p_{0.5} \approx 2$ across the inertial range. Newer data from Sreenivasan in the atmospheric boundary layer (private communication) are included in figure 2(b), and show variation with scale.

To get a clearer view of the cause of this variation, the pdfs of the breakdown coefficients $q_{\Delta x}$ of a 'parent' segment of length Δx were conditioned not only on Δx, but also on its integrated dissipation, which is expressed for convenience as a surrogate velocity difference

$$\delta u = (\varepsilon_{\Delta x}\Delta x)^{\frac{1}{3}}. \tag{4.3}$$

The conditioning cells are spaced logarithmically in both variables, by a factor of 2 in Δx, and by $\sqrt{2}$ in δu. The result is a two-dimensional array of pdfs, each of which can be characterized by its maximum. Contour plots of the distribution of the conditional $p_{0.5}$ are given in figure 3 for two Reynolds numbers. Both plots have been scaled so that the Kolmogorov length maps to zero in the abscissae, and the integral length maps to 1.5. The abscissae 0.5 corresponds to the Taylor microscale λ. In the ordinates, zero corresponds to the large-scale fluctuation intensity u', and -1 to the Kolmogorov velocity scale $u_K = \nu/\eta$. The dashed diagonal line in each plot therefore represents
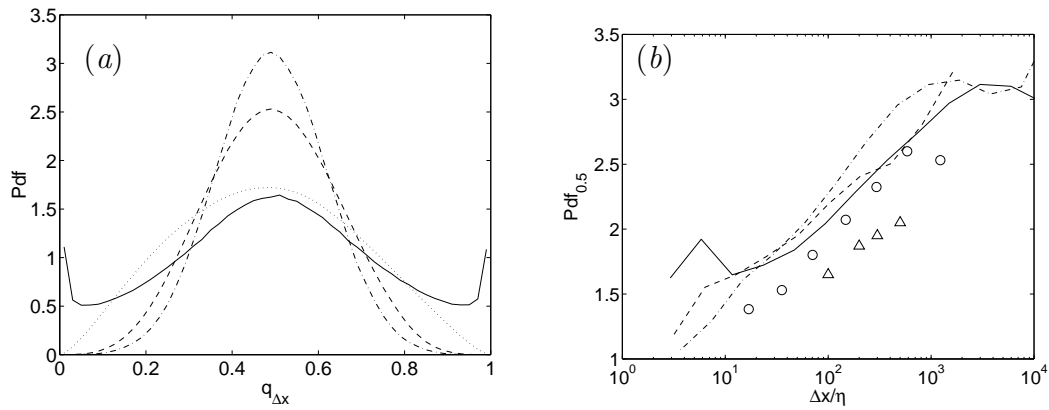
Figure 2.- (*a*) Pdfs of the breakdown coefficients of the surrogate averaged dissipation, for several averaging lengths. $Re_\lambda = 1600$. ——— , $\Delta x/\eta = 3$; ········ , 24; - - - - , 380; —·— , 3000. (*b*) Midpoint value of the pdf as a function of averaging length. Lines are as in table 1; ○ , Van Atta and Yeh (1975). $Re_\lambda = 2600$; △ , Sreenivasan (private communication). $Re_\lambda = 15,000$.
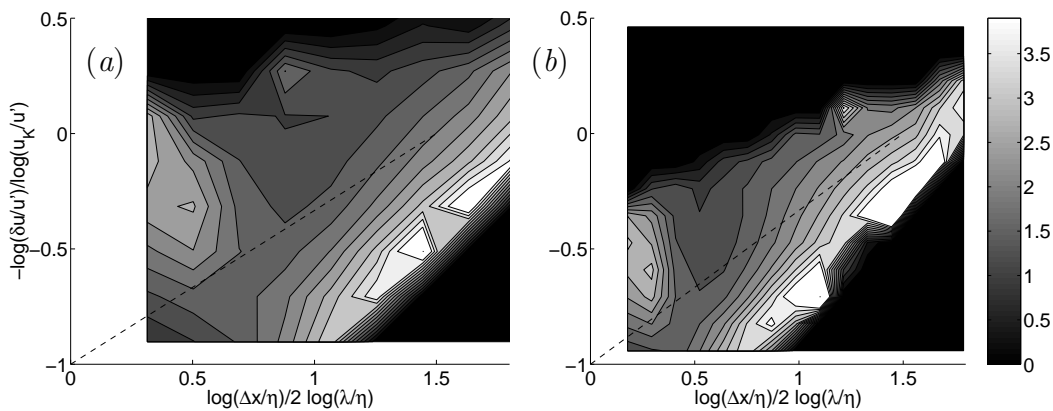

Figure 3.- Midpoint value of the conditional pdfs of the breakdown coefficients for the surrogate averaged dissipation, as a function of the averaging length and of the surrogate velocity increment. (*a*) $Re_\lambda = 155$. (*b*) $Re_\lambda = 1600$.

the usual Kolmogorov cascade, $\delta u = (\varepsilon \Delta x)^{\frac{1}{3}}$. The black areas in the plots do not label cases in which the maximum value of the pdf vanishes, but cells for which there are not enough data to compile statistics. Not surprisingly, the cells containing more data cluster around the classical Kolmogorov line.

The behaviour of $p_{0.5}$ is the same in both cases. The distributions of the breakdown coefficients of weaker fluctuations are, for a given length scale, more concentrated about the mean than those of stronger ones, and therefore
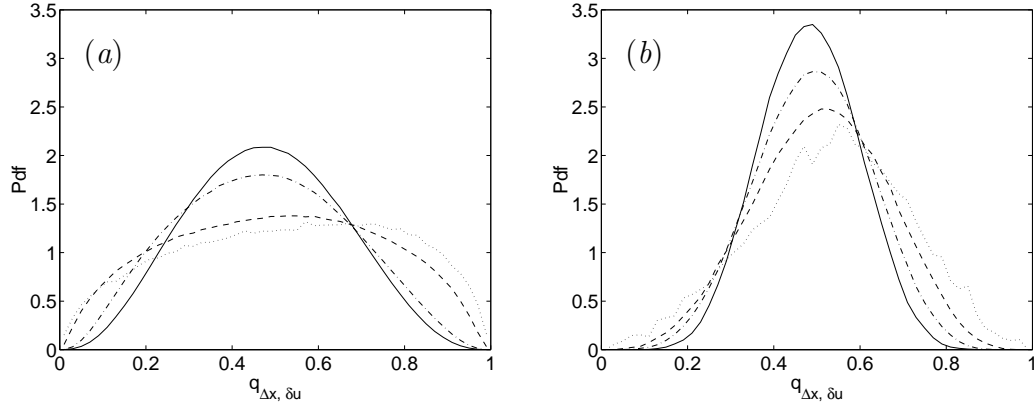
Figure 4.- Conditional pdfs of the dissipation breakdown coefficients, for several dissipations and length scales. $Re_\lambda = 1600$. (a) $\Delta x/\eta = 23$, corresponding to an abscissa of 0.5 in figure 3. Dissipations correspond to the following ordinates in figure 3: —— , -0.94; —·— , -0.82; ---- , -0.59; ········ , -0.36. (b) $\Delta x/\eta = 1500$ (abscissa, 1.2). Ordinates: —— , -0.36; —·— , -0.24; ---- , -0.12; ········ , 0.

have higher maxima. Concentrated distributions are the result of uncorrelated random processes. The integrated dissipation (4.1) is a sum of variables and, in the simplest hypothesis that the dissipation is only coherent over distances of the order of the Kolmogorov scale, it is easy to show that the distributions of $\varepsilon_{\Delta x}$ and of q should quickly become approximately Gaussian, with maxima increasing as $(\Delta x/\eta)^{\frac{1}{2}}$. The same conclusion would follow from a model in which a limited number of strong isolated small-scale structures account for the bulk of the dissipation. That this is not true is clear from figure 2(b), where the maxima increase only logarithmically with Δx, suggesting the presence of structure in the velocity field at all scales.

Low maxima and wide distributions are the results of coherence, or at least of local statistical inhomogeneity, since the distribution of the dissipation over the two halves of a segment Δx can take any value depending on where the mid-point lies with respect to the inhomogeneous structure. Over most of the plots in figure 3 is it clear that weaker fluctuations break more randomly, while stronger ones break more coherently. The pattern is apparently reversed for distances in the dissipative range, but this can be shown to be due to a different effect. The dissipation is effectively constant over those distances, and segments are again most likely to contain one half of the dissipation of their parents. In fact the dissipative distributions tend to be trimodal, with a larger peak at $q = 0.5$ and weaker ones at $q = 0$ and $q = 1$.

Some examples of conditioned inertial pdfs are shown in figure 4. All the distributions are roughly bell-shaped, but those which correspond to very

strong structures over short distances are almost flat, suggesting a breakdown into random subintervals of single structures with sizes comparable to that of the averaging segment. Note that the distributions are not exactly symmetric. While the most probable value for the dissipation of the central half of a weak fluctuation is weaker than that of its parent, that of of a strong fluctuation tends to be stronger.

This lack of universality of the breakdown coefficients weakens the experimental support for the the self-similar cascade models, but it does not completely disprove them. It has been noted in several occasions that the integrated dissipation is not a good quantity on which to base a local cascade theory since, in the first place, it only represents the energy transfer rate in an averaged sense and, in any case, the transfer rate is itself not a local quantity. It is easy to see from simple dimensional considerations that the spatial energy fluxes are of the same order as the energy transfer to smaller scales, and that the kinetic energy of a fluid volume is as likely to diffuse to a neighbouring structure of roughly the same scale, as to decay into smaller structures (see e.g. the discussion in Jiménez 1999). An experimentally confirmed consequence is that the local energy transfer to subgrid can be positive or negative with comparable probabilities (Piomelli *et al.* 1991).

4.1   The scaling exponents

That the pdfs of the breakdown coefficients are not found to be universal raises the question of why reasonably good power laws are experimentally found for the moments of the dissipation and for the structure functions of the velocity increments.

In the multiplicative model, and subject only to the statistical independence of consecutive cascade steps, the moments of the dissipation after n steps can be expressed as products of the moments of individual breakdown coefficients and, if we assume that Kolmogorov's detailed similarity hypothesis is satisfied, the scaling exponents of the structure functions of the absolute values of the velocity increments are given by (Frisch 1994)

$$S_p = \langle |\Delta u|_{\Delta x}^p \rangle \sim \Delta x^{\zeta_p}, \qquad \zeta_p = -\frac{1}{3} \log_2 \langle q_{\Delta x}^p \rangle, \qquad (4.4)$$

where,

$$\Delta u_{\Delta x} = u(x + \Delta x/2) - u(x - \Delta x/2). \qquad (4.5)$$

The logarithm in (4.4) is one of the reasons why the slopes ζ_p appear to be relatively constant in experiments, even if the underlying distributions are not. Another reason, already noted by Sreenivasan and Stolovitzky (1995) and by Nelkin and Stolovitzky (1996), is that moments are poor indicators of the shape of probability distributions of bounded variables. The bell-shaped
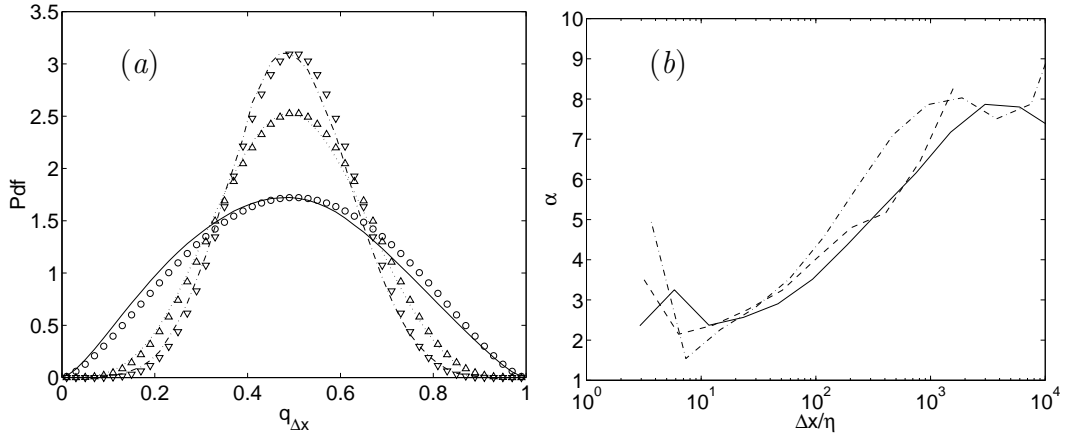
Figure 5.- (*a*) Approximation of the experimental pdfs of the dissipation breakdown coefficients by symmetric Beta distributions having the same maxima. $Re_\lambda = 1600$. ——— , $\Delta x/\eta = 23$; ········· , 370; —·— , 6000. (*b*) Best value of α for the Beta approximation of the breakdown pdfs. Lines as in table 1.

functions in figure 2(*a*) can be approximated by Beta distributions,

$$p_\alpha(q) = \frac{q^{\alpha-1}(1-q)^{\alpha-1}}{B(\alpha, \alpha)}, \tag{4.6}$$

where $B(\alpha, \alpha)$ is the Beta function, and $\alpha \approx 4 - 8$ (see figure 5). The *p*-th moment of (4.6) is

$$\langle q_{\Delta x}^p \rangle = \frac{B(\alpha + p, \alpha)}{B(\alpha, \alpha)}, \tag{4.7}$$

and is given, in the form of ζ_p, by the solid lines in figure 6(*a*). They are relatively insensitive to α in the range of interest, but they would still give a noticeable curvature in a logarithmic plot of S_p against Δx. A procedure to obtain better power laws was introduced by Benzi *et al.* (1993), by plotting S_p not against Δx (or α in our case), but against ζ_3, which should theoretically scale linearly with Δx in an ideal inertial range. This is equivalent to substituting the scaling exponents by

$$\zeta_p' = \zeta_p/\zeta_3, \tag{4.8}$$

and has often been used since then to analyze experiments. These extended exponents are given as dashed lines in 6(*a*), and are even less sensitive than ζ_p to variations in α. Finally the results of (4.8) are compared in figure 6(*b*) with experimental data, with reasonable results.

It should be emphasized how little this subsection has to do with physics. Its only input is that the pdfs of the breakdown coefficients are approximately
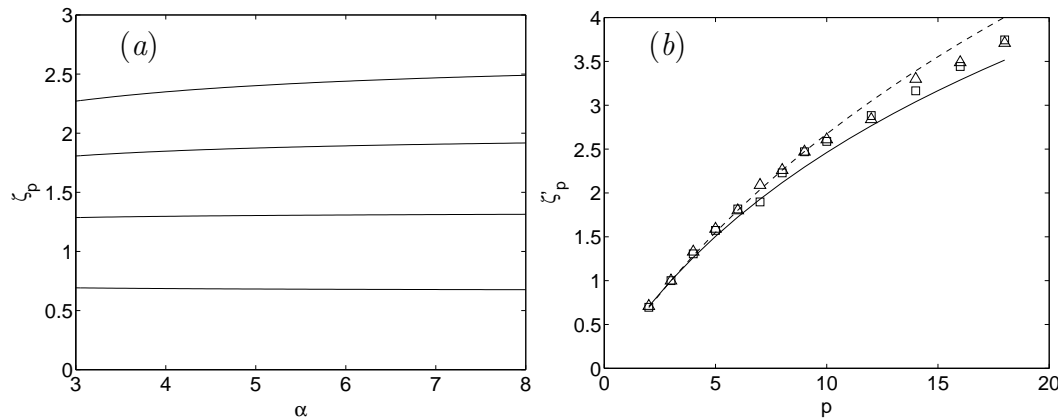
Figure 6.- (*a*) Scaling exponents for the Beta distributions, as a function of the parameter α. $p = 2, 4, 6, 8$, in increasing order. ——— , true exponent; - - - - , extended self-similarity. (*b*) Scaling exponents of the longitudinal velocity structure functions. □ , Herweijer and van de Water (1994); △ , Anselmet *et al.* (1984). $Re_\lambda \approx 500 - 800$ in both cases; ——— , Beta distribution with $\alpha = 5$; - - - - , $\alpha = 8$.

bell-shaped, even if their maxima change by more than a factor of two in the scales being considered, but it ends with the analytic formula (4.4)–(4.7) for the scaling exponents. It was noted by Sreenivasan and Stolovitzky (1995) that similar results can be achieved with even less information.

Our purpose in this case cannot be to explain the physics of the cascade, even if we have already observed that there is some physical information in the relatively slow variation of the pdfs with the length scale, but to emphasize once more the insensitivity of the scaling exponents as a tool for this purpose. It can be noted in passing that the extended self-similarity procedure appears in this light as essentially a mathematical artifact, which hides, rather than highlights, the underlying physical processes.

5   The velocity increments

To get more information on the inertial range than was possible from the coarse-grained dissipation, we now consider directly the velocity increments (4.5). It is unfortunately difficult to study them from the point of view of multiplicative cascades since they are not intrinsically positive and their most probable value is close to zero. It is easier to compute directly the joint probability function of the velocity increments at different scales, which contains the full two-point statistical information. The multiplicative cascade is just a particular model for this object. As in the previous section we will consider
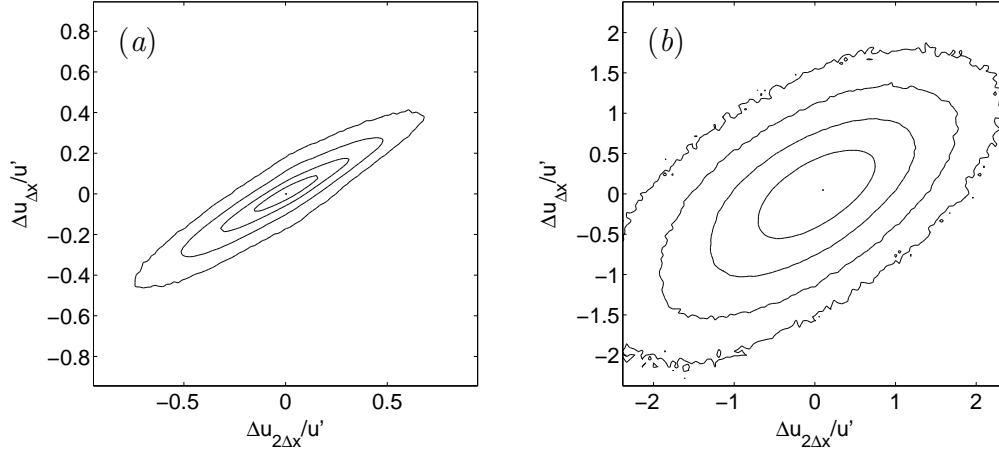
Figure 7.- Joint pdfs of the velocity increments across centred segments whose lengths differ by a factor of two. $Re_\lambda = 1600$. (a) $\Delta x/\eta = 6$. (b) $\Delta x/\eta = 90$. Contour lines are logarithmically spaced by factors of 10.

centred segments whose lengths differ by a factor of two. The joint pdfs of the velocity increments were recently studied by Friedrich and Peinke (1997), who showed that they are consistent with a Markovian cascade characterized by a drift, depending linearly on the parent velocity difference, and by an additive noise with a parabolic variance. They analyzed data from the centreline of a jet at $Re_\lambda \approx 600$, and their pdfs look similar to those in figure 7, which belong to our highest Reynolds number case. They are not Gaussian, and the correlation coefficient of the two increments, which is roughly proportional to the elongation of the ellipses, depends on the scale. It is given for our three data sets by the symbols in figure 8(a). It is close to unity for very short scales, and decays to almost zero near the integral length. For the higher Reynolds numbers the correlation has a plateau in a range that roughly coincides with the inertial range.

While that plateau looks interesting, it says more about our data analysis than about the structure of the flow. The reason for using velocity differences is to isolate particular length scales, which means that the difference operator is being used as a band-pass filter. As such it is far from ideal. If we consider the Fourier transform $\widehat{u}(k)$ of the velocity, any homogeneous linear operator multiplies $\widehat{u}$ by a transfer function which, in the particular case of (4.5), is

$$\widehat{\Delta u}/\widehat{u} = F(k\Delta x) = 2\mathrm{i}\sin(k\Delta x/2). \tag{5.1}$$

It follows from Parseval's theorem that the covariance of two functions can be written in terms of their cospectrum

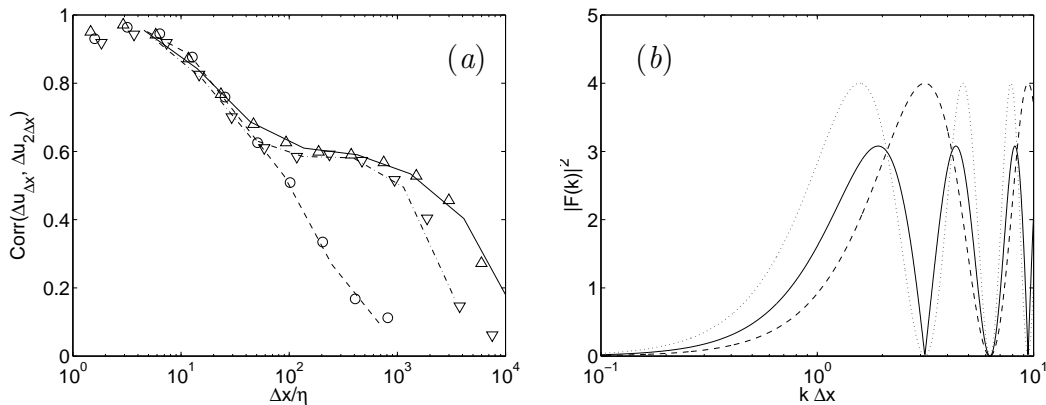$$\langle uv \rangle = \Re \int_0^\infty \widehat{u}\widehat{v}\,\mathrm{d}k, \tag{5.2}$$

Figure 8.- (a) Correlation coefficients for the joint pdfs in figure 7, as a function of the separation distance. Lines are as in table 1. (b) Transfer functions for the difference operator. $----$, $|F(k\Delta x)|^2$; $\cdots\cdots$, $|F(2k\Delta x)|^2$; ——— , $|F(k\Delta x)F^*(2k\Delta x)|$.

which, for two velocity differences, takes the form

$$\langle \Delta_1 u \, \Delta_2 u \rangle = \int_0^\infty \Re\{F(k\Delta_1 x)F^*(k\Delta_2 x)\}E(k)\,\mathrm{d}k, \qquad (5.3)$$

where the asterisk stands for complex conjugation and $E(k)$ is the energy spectrum of u. Since the variance of each velocity difference can also be computed in terms of spectrum and of the transfer function,

$$\langle \Delta u^2 \rangle = \int_0^\infty |F(k\Delta x)|^2 E(k)\,\mathrm{d}k, \qquad (5.4)$$

the correlation coefficient

$$\mathrm{Corr}(\Delta_1 u \, \Delta_2 u) = \langle \Delta_1 u \, \Delta_2 u \rangle / \left(\langle \Delta_1 u^2 \rangle \langle \Delta_2 u^2 \rangle \right)^{\frac{1}{2}}, \qquad (5.5)$$

can be expressed solely in terms of the spectrum and of the filter. The key quantity is the overlap of the two transfer functions, which appears in (5.3). If the band-pass filters are narrower than the separation of the two filter widths, the correlation of the filtered velocities is small while, in the opposite case, it is large. The magnitude of (5.1) at separations spaced by a factor of two is given in figure 8(b), together with their product. The overlap is substantial, and the product has a wide support, implying that the correlation seen in figure 8(a) is mostly due to inadequacy of our filtering scheme. The lines in figure 8(a) are computed using (5.1)–(5.4) and the measured velocity spectra.

While the previous discussion is elementary, it should caution us against reading too much physics into the properties of the velocity differences since, at least in part, they may be due to the spectral spillage between different separation scales.
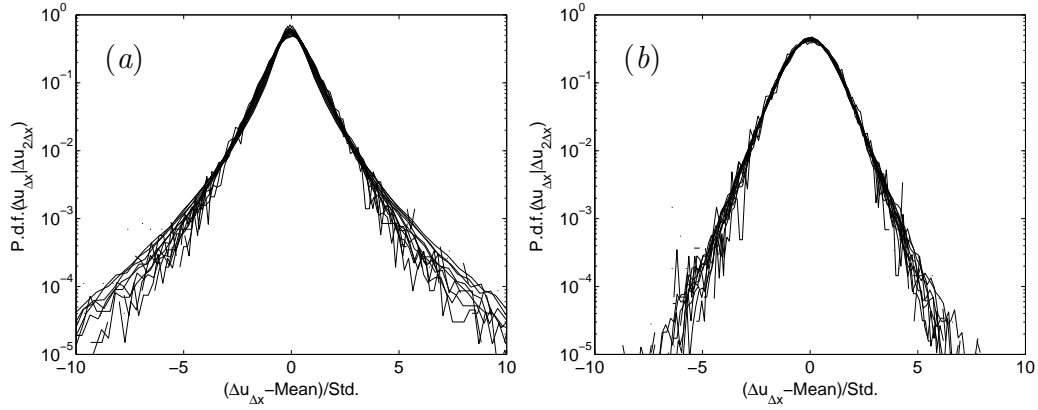
Figure 9.- Normalized pdfs of $\Delta u_{\Delta x}$ conditioned on the velocity increment $\Delta u_{2\Delta x}$ of its parent interval. $Re_\lambda = 1600$. (a) $\Delta x/\eta = 12$, $|\Delta u_{2\Delta x}/u_K| = 1 - 14$. ($b$) $\Delta x/\eta = 750$, $|\Delta u_{2\Delta x}/u_K| = 4 - 60$.
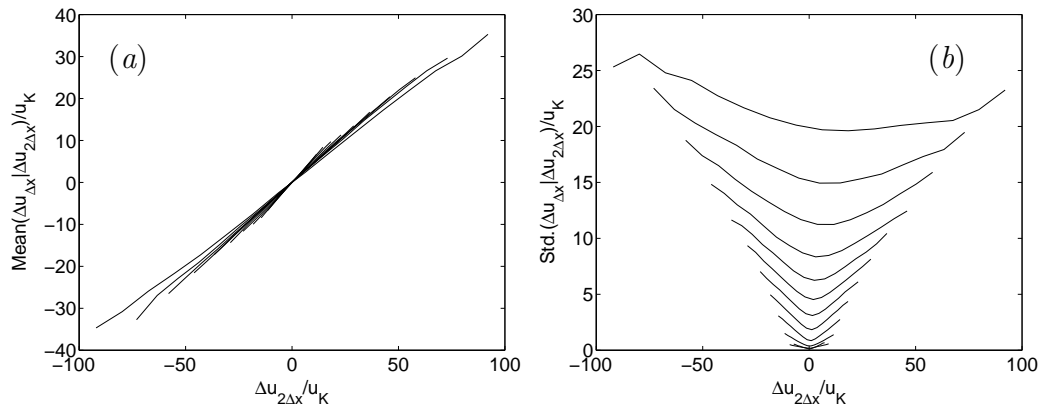

Figure 10.- (a) Mean value of $\Delta u_{\Delta x}$, conditioned on the velocity increment $\Delta u_{2\Delta x}$ of its parent interval. (b) Standard deviations. In both figures $\Delta x/\eta$ ranges from 1.5 to 3000, increasing by factors of 2 in the direction of longer lines. $Re_\lambda = 1600$.

Consider for example the conditional pdfs of $\Delta u_{\Delta x}$, conditioned on the value of $\Delta u_{2\Delta x}$, some of which are given in figure 9. It is interesting that, once normalized with their own mean and standard deviation, they approximately collapse for a given Δx, independently of the conditioning velocity. They are however not Gaussian, and their shape depends on Δx, being more intermittent for the smaller scales, and looking generally similar to the global pdfs of the velocity increments at the same length scale. Their conditional means and standard deviations are shown in figure 10, where each line corresponds to a given Δx, and where the quantities are plotted against the conditioning velocity difference. Note that the local self-similarity hypothesis
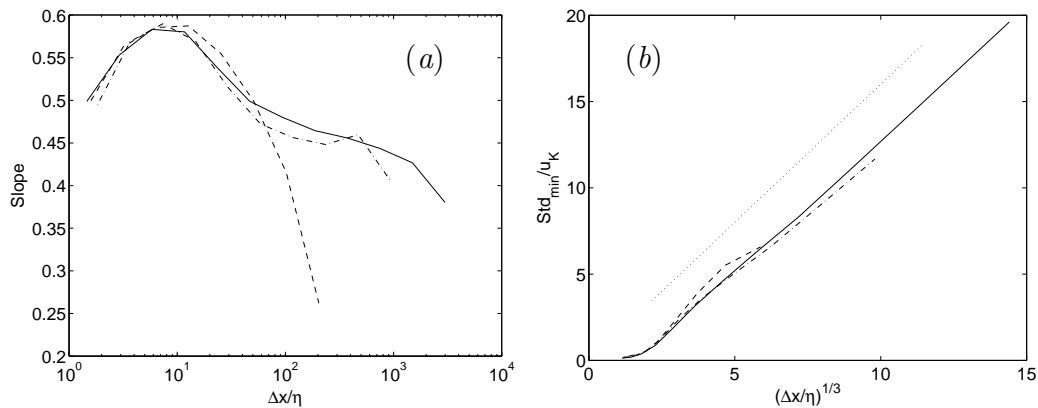
Figure 11.- (a) Slope of the conditional mean values in figure 10(a), $\mathrm{d}\langle\Delta u_{\Delta x}|\Delta u_{2\Delta x}\rangle/\mathrm{d}\Delta u_{2\Delta x}$. ($b$) Minimum conditional standard deviations in figure 10(b). Lines as in table 1. The slope of the dotted line is 1.6.

for the cascade would imply that both the mean and the standard deviations should be proportional to the conditioning $\Delta u_{2\Delta x}$, and that, while this is approximately true for the former, it is not for the latter. This was also noted by Friedrich and Peinke (1997), and implies that self similarity is incomplete, as discussed in §2, and that the weak perturbations are dominated by background fluctuations.

The minimum value of the conditional standard deviations for each Δx is plotted in figure 11(b), and is proportional to the Kolmogorov velocity at that scale $(\varepsilon\Delta x)^{1/3}$. The slope of the conditional mean with respect to the conditioning velocity is given in 11(a), and is close to 0.5, as it would be for the velocity differences of a smooth variable. This suggests that the behaviour of the mean is a property of the filtering procedure rather than intrinsic to the velocity, which is not smooth at inertial scales. It is indeed easy to construct filters whose band-pass characteristics are sharp enough for the correlation of the filtered velocities to be much smaller than for the increments. We will discuss one such filter below, and we will see that the slope of the mean values can be made very small, or even negative, while the behaviour of the standard deviations is robust. Note that the deviations of both the mean and the standard deviation from their 'inertial' values collapse well in Kolmogorov variables across different Reynolds numbers, and that there is no indication of other scales, such as the Taylor microscale, being important for the behaviour of the pdfs.

The parabolic shape of the standard deviations in figure 10(b) suggests that the cascade process can be understood in terms of two processes. The random background noise discussed in the previous paragraph, and a more deterministic process which generates 'coherent' fluctuations which are proportional
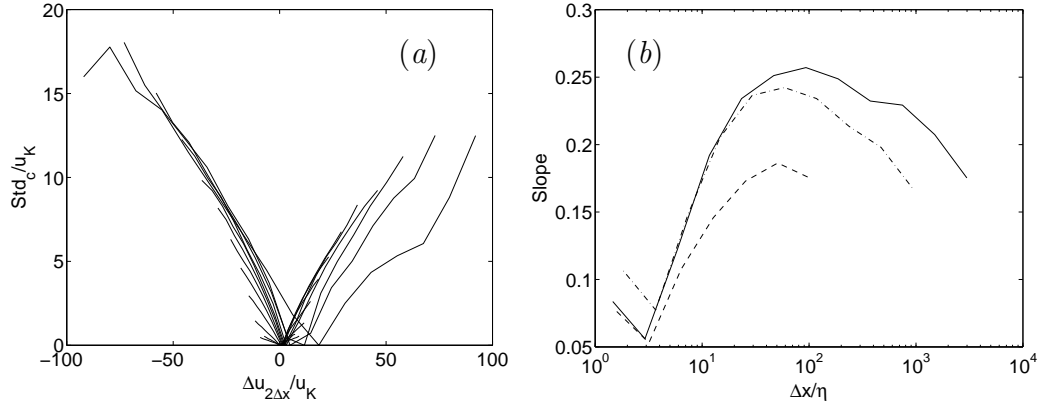
Figure 12.- (a) 'Coherent' conditional standard deviation of the velocity increments, as a function of the conditioning velocity increments. Data as in figure 10. Each line represents a different Δx. $Re_\lambda = 1600$. (b) Slope of the coherent standard deviation in (a) with respect to the conditioning velocity increments. Lines as in table 1. The slopes of the positive and negative branches of (a) have been averaged for this figure.

to those in the parent interval. Assuming both processes to be independent, their variances add, and we can define a coherent standard deviation for the second process

$$\mathrm{Std}_c = \left(\mathrm{Std}^2 - \mathrm{Std}_{min}^2\right)^{\frac{1}{2}}. \tag{5.6}$$

This is plotted in figure 12(a), and indeed varies approximately linearly with the parent velocity increment. Its slope, for our three data sets, is plotted in 12(b) as a function of the interval length. At least for the two higher Reynolds numbers it has a plateau at roughly 0.25 at the inertial scales, and falls to very low values in the dissipative range, as the flow becomes smooth and its stochastic component disappears. The location of the decay, $10 - 20\eta$ roughly corresponds to the end of the power-law behaviour in the energy spectrum.

5.1   Sharper filters

We have noted that the properties of the velocity difference as a band-pass filter are far from ideal, which led to some spurious properties of the joint statistics of increments at different length scales. Sharper filters, with less spectral leakage, can be constructed, but generally need to use velocities from more points than the two used in (4.5), and they are most effective when tuned to a particular energy spectrum. In this section we will consider the next simplest filter, using four instead of two points. It can be written in the
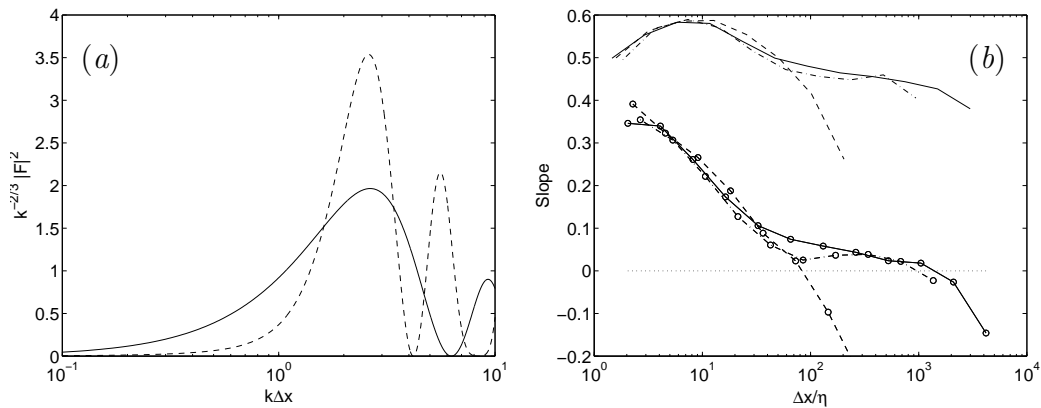
Figure 13.- (a) Filtered inertial spectra $kE(k)|F(k)|^2$, with $E = k^{-5/3}$. —— , for the difference operator (4.5); ---- , for the 'sharp' filter (5.7). (b) Slope of the conditional mean values. Simple lines are the same as in figure 11(a). Those with symbols are computed with (5.7).

general form

$$\widetilde{\Delta}u = a\left[u(x + \widetilde{\Delta}x/2) - u(x - \widetilde{\Delta}x/2)\right] - ab\left[u(x + \widetilde{\Delta}x) - u(x - \widetilde{\Delta}x)\right], \quad (5.7)$$

where the parameters a, b and p can be adjusted to get the desired transfer function. We will use

$$a = 1.075, \qquad b = 0.4, \qquad \widetilde{\Delta}x = \frac{3}{2}\Delta x, \qquad (5.8)$$

which are chosen so that the peak of the transfer function is at the same location as in (5.1), and the correlation (5.3) vanishes when applied to an inertial power spectrum $E(k) = k^{-5/3}$ (see figure 13-a). Note that, if (4.5) is a discrete approximation to the velocity gradient, (5.7), with the coefficients in (5.8), is very close to a discrete third derivative, and that it is also possible to think of it as an orthogonal wavelet basis in which orthogonality is defined by the integral in (5.3) with a weighting function which is the energy spectrum (Farge 1992)

When the analysis in the previous section is applied to velocities filtered in this way, instead of to the velocity differences, the general shape of the joint pdfs is the same, but the correlation of $\widetilde{\Delta}u_{\Delta x}$ and $\widetilde{\Delta}u_{2\Delta x}$ vanishes, and the slope of the conditional means is now much smaller than before, and even reverses in sign for the largest scales (figure 13-b).

Other properties are more robust. The standard deviations of the conditional probabilities have the same general behaviour as in the previous case. Its incoherent part is still proportional to the background fluctuation intensity, although with a slightly higher numerical factor, $\text{Std}_{min}(\varepsilon\Delta x)^{-1/3} \approx 1.8$,

rather than the 1.6 in figure 11(b). A coherent part can also be defined, and it also depends approximately linearly on the filtered velocity of the parent interval, with a proportionality coefficient that reaches a plateau beyond $\widetilde{\Delta}x/\eta \approx 10$, as in figure 12($b$), but which is now 0.3 instead of 0.25.

6 Discussion and conclusions

We have analyzed longitudinal velocity signals from three different data sets of approximately isotropic turbulence at low to moderate Reynolds numbers, the highest of which contains a well-developed inertial range over almost three decades. The classical analysis of the scaling of the coarse-grained dissipation does not support the often quoted assumption that the pdfs of the breakdown coefficients are universal in the inertial range, although their variation with scale is much slower than would correspond to a completely uncorrelated dissipation field.

A classification of the pdfs in terms of the length scale and of the dissipation of the parent interval shows the structure of the cascade, which is given in figure 2. Weaker fluctuations at each length scale break according to concentrated distributions, which correspond to uncorrelated processes, while stronger ones break more coherently, with broader pdfs. That separation becomes stronger at the smaller scales.

This interpretation, which is consistent with the theoretical ideas, summarized in §2, of how the strong fluctuations should decouple from the background, are confirmed by the conditional pdfs in §5, which are conditioned on the velocity increment of the parent interval. They do not support full self-similarity of the cascade, because the standard deviations of the 'children' increments are not proportional to the magnitude of their 'parents'. This is however approximately true of the stronger fluctuations, and the distributions can be separated into two components. A weaker one, which is dominated by the background, and whose standard deviation is independent of the intensity of the parent interval, and a stronger one, whose standard deviation is proportional to that intensity. The proportionality constant (~ 0.25) is approximately constant through the inertial range.

The velocity scale separating the two ranges is the Kolmogorov velocity at the particular length scale, $u'_{\Delta x} = (\varepsilon \Delta x)^{1/3}$. This contradicts the earlier assumption by Jiménez and Wray (1998), who had guessed that the relevant scale was the r.m.s. vorticity magnitude at the Kolmogorov scale $(\varepsilon/\nu)^{1/2}$, and implies that there is no preferred length scale in the cascade except for the Kolmogorov and the integral scales that bound it. The Reynolds number scaling of the observed distributions is consistent with this conclusion. It cannot however be concluded from the present statistics whether the intermittent structures form a self-similar continuum across the inertial range, or are simply the reflection of the known coherence at the integral and Kolmogorov

scales.

Another self-similar property, that of the mean values of the conditional distributions, was traced to the poor performance of the velocity increments as band-pass filters. It disappears when a sharper filter is used, but the behaviour of the standard deviation is robust.

We have also noted that the lack of self-similarity found for the breakdown distributions is consistent with the experimentally observed approximate power-law behaviour of the structure functions, and we have stressed, once more, that the latter are poor indicators of the self-similarity of the underlying processes, and should be used with care. We have shown this by computing the scaling exponents from a simple parametric approximation to the observed pdfs, and observed that, in this light, the better power laws obtained from extended self-similarity should be seen as hiding, rather than illuminating, the underlying physics of the cascade.

It should in any case be stressed that the analysis presented here, as most similar ones, is essentially kinematic, describing the state of the flow at a given time, and should not be confused with a dynamical description of a possible cascade process, which would require the study of the time evolution of individual structures.

References

Anselmet, F., Gagne, Y., Hopfinger, E.J., Antonia, R.A. (1984) 'High-order structure functions in turbulent shear flow', *J. Fluid Mech.* **140**, 63–89.

Batchelor, G.K., Townsend, A.A. (1949) 'The nature of turbulent motion at large wave numbers', *Proc. Roy. Soc. Lond. A* **199**, 238–255.

Belin, F., Maurer, J., Tabeling, P., Willaime, H. (1997) 'Velocity gradient distributions in fully developed turbulence: experimental study', *Phys. Fluids* **9**, 3843–3850.

Benzi, R., Ciliberto, S., Tripiccione, R., Baudet, C., Massaioli, F., Succi,S. (1993) 'Extended self-similarity in turbulent flows', *Phys. Rev.* **48**, R29–R32.

Brown, G.L., Roshko, A. (1974) 'On the density effects and large structure in turbulent mixing layers', *J. Fluid Mech.* **64**, 775–816.

Chhabra,A.B., Sreenivasan,K.R. (1992) 'Scale–invariant multiplier distributions in turbulence', *Phys. Rev. Lett.* **68**, 2762–2765.

Farge, M. (1992) 'Wavelet transforms and their application to turbulence', *Ann. Rev. Fluid Mech.* **24**, 395–457.

Friedrich, R., Peinke, J. (1997) 'Description of a turbulent cascade by a Fokker-Plank equation', *Phys. Rev. Lett.* **78**, 863–866.

Frisch, U. (1995) *Turbulence. The legacy of A.N. Kolmogorov.* Cambridge U. Press.

Gurvich, A.S., Yaglom, A.M. (1967) 'Breakdown of eddies and probability distributions for small-scale turbulence, boundary layers and turbulence', *Phys. Fluids Suppl.* **10**, S 59–65.

Herweijer, J.A., van de Water, W. (1995) 'Universal shape of scaling functions in turbulence', *Phys. Rev. Lett.* **74**, 4651–4654.

Hosokawa, I., Oide, S., Yamamoto, K. (1997) 'Existence and significance of 'soft worms' in isotropic turbulence', *J. Phys. Soc. Japan* **66**, 2961–2964.

Jiménez, J. (1998) 'Small scale intermittency in turbulence', *Eur. J. Mech. B/Fluids* **17**, 405–419.

Jiménez, J. (1999) 'Self-similarity and coherence in the turbulent cascade', in *Proc. IUTAM Symp. Geometry and Statistics of Turbulence*, Hayama, Japan, Nov. 1–5, 1999.

Jiménez, J. (2000) 'Intermittency and cascades', *J. Fluid Mech.* **409**, 99–120.

Jiménez, J., Wray, A.A. (1998) 'On the characteristics of vortex filaments in isotropic turbulence', *J. Fluid Mech.* **373**, 255–285.

Jiménez, J., Wray, A.A., Saffman, P.G., Rogallo, R.S. (1993) The structure of intense vorticity in isotropic turbulence, *J. Fluid Mech.* **255**, 65–90.

Kolmogorov, A.N. (1941) 'The local structure of turbulence in incompressible viscous fluids a very large Reynolds numbers', *Dokl. Akad. Nauk. SSSR* **30**, 301–305.

Kolmogorov, A.N. (1962) 'A refinement of previous hypotheses concerning the local structure of turbulence in a viscous incompressible fluid at high Reynolds number', *J. Fluid Mech.* **13**, 82–85.

Meneveau, C., Sreenivasan, K.R. (1991) 'The multifractal nature of the energy dissipation', *J. Fluid Mech.* **224**, 429–484.

Moisy, F., Tabeling, P., Willaime, H. (1999) 'Kolmogorov equation for a fully developed turbulence experiment', *Phys. Rev. Lett.* **82**, 3994–3997.

Nelkin, M. (1994) 'Universality and scaling in fully developed turbulence', *Adv. Physics* **43**, 143–181.

Nelkin, M., Stolovitzky, G. (1996) 'Limitations of random multipliers in describing turbulent energy dissipation', *Phys. Rev. E* **54**, 5100–5106.

Novikov, E.A. (1971) 'Intermittency and scale similarity in the structure of a turbulent flow', *Prikl. Mat. Mech.* **35**, 266–277. Translated in *Appl. Math. Mech.* **35**, 231–241.

Novikov, E.A. (1990) 'The effect of intermittency on statistical characterization of turbulence and scale similarity of breakdown coefficients', *Phys. Fluids A* **2**, 814–820.

Piomelli,U., Cabot,W.H., Moin,P., Lee,S. 1991 'Subgrid-scale backscatter in turbulent and transitional flows'. *Phys. Fluids A* **3**, 1766–1771.

Porter, D.H., Woodward, P.R., Pouquet, A. (1998) 'Inertial range structures in decaying compressible turbulent flows', *Phys. Fluids* **10**, 237–245.

Richardson, L.F. (1922) *Weather prediction by numerical process*, p. 66, Cambridge U. Press, reprinted by Dover.

Siggia, E.D. (1981) 'Numerical study of small scale intermittency in three dimensional turbulence', *J. Fluid Mech.* **107**, 375–406.

Sreenivasan, K.R., Stolovitzky, G. (1995) 'Turbulent cascades'. *J. Stat. Phys.* **78**, 311-333.

Tabeling, P., Zocchi, G., Belin, F., Maurer, J., Willaime, H. (1996) 'Probability density functions, skewness and flatness in large Reynolds number turbulence', *Phys. Rev. E* **53**, 1613–1621.

Van Atta, C. W., Yeh, T.T. (1975) 'Evidence for scale similarity of internal intermittency in turbulent flows at large Reynolds numbers', *J. Fluid Mech.* **71**, 417–440.

Zocchi, G., Tabeling, P., Maurer, J., Willaime, H. (1994) 'Measurement of the scaling of the dissipation at high Reynolds numbers', *Phys. Rev. E* **50**, 3693–3700.